Numerical treatment of boundary conditions to replace lateral branches in haemodynamics

Porpora A., Zunino P., Vergara C., Piccinelli M.

Numerical treatment of boundary conditions to replace lateral branches in haemodynamics [*]

Azzurra Porpora[†], Paolo Zunino[‡], Christian Vergara[§], Marina Piccinelli[¶]

Abstract

In this paper, we discuss a technique for weakly enforcing flow rate conditions in computational hemodynamics. In particular, we study the effectiveness of cutting lateral branches from the computational domain and replacing them with non perturbing boundary conditions, in order to simplify the geometrical reconstruction and the numerical simulation. All these features are investigated both in the case of a rigid and of a compliant wall. Several numerical results are presented in order to discuss the reliability of the proposed method.

1 Introduction and motivations

The prescription of suitable boundary conditions on artificial sections is a major issue in computational haemodynamics [27]. An artificial section is a part of the domain boundary which does not correspond to any physical wall, but it is just introduced by the truncation of the computational domain, in order to separate a vascular district selected for a computational fluid-dynamics (CFD) analysis from the proximal and distal parts of the arterial tree [15].

In the last years, the development in the biomedical acquisition techniques, such as phase contrast-magnetic resonance imaging (PC-MRI), allowed to obtain satisfying pointwise information about the velocity field at a section. However, these procedures are nowadays still very onerous both from computational (3-4 minutes are needed for each acquisition, which often has to be repeated), and economic point of view.

For this reason, a great attention in computational haemodynamics is still paid to averaged data, which can be more easily obtained, for example with a Doppler-ultrasound technique, which unlike MRI is very fast and inexpensive.

In particular, with this technique it is possible to obtain at each time the *flow rate*

$$Q = \int_\Gamma \boldsymbol{u} \cdot \boldsymbol{n} \, ds,$$

where $\boldsymbol{u}$ is the fluid velocity, Γ the section at hand, and $\boldsymbol{n}$ the unit outward normal. When such data are prescribed as boundary conditions at the artificial sections, they are usually referred as *defective* boundary conditions, because some additional requirement is needed to close the system of governing equations.

Another situation where averaged data are needed is when one couples the 3D model with reduced models (one-dimensional, 1D, or zero-dimensional) to take into account the complementary part of the arterial tree. In this case, due to the reduced dimensionality of such models, just averaged quantities, such as the flow rate, can be exchanged with the 3D model. We refer the interested reader to [11] for a review of these topics.

Several strategies have been introduced for the management of defective flow rate conditions. The first *ad hoc* treatment is found in [15], where the authors proposed a suitable variational formulation, which however requires to build up null-flow rate functional spaces, which are hardly discretized by means of the finite element method. For this reason, other techniques have been developed in the last decade. We cite the Lagrange multipliers approach [10, 30, 31], an optimal control-based method [12], and the coupled momentum method [33, 34]. Recently, in [37] the authors proposed to manage the flow rate condition through Nitsche's method [23]. This method does not introduce additional unknowns such as Lagrange multipliers and it does not need any iterative schemes to solve the discrete problem as in the optimal control-based approach (for a numerical comparison with the Lagrange multipliers technique, see [32]). When applied to flow rate conditions, Nitsche's technique weakly perturbs the flow profile naturally determined by the continuity and momentum equations inside the computational domain. However, a weak boundary control can lead to lack of stability of the numerical scheme. On this basis, the analysis of [5, 8, 20] is devoted to develop and compare numerical treatments of outflow boundary conditions to avoid backflow effects that could destabilize the numerical scheme. Such obstacle will be overridden by means of a suitable stabilization technique.

In this work, we consider Nitsche's method for the prescription of defective conditions applied to haemodynamics. More precisely, the main goal of this work is to study its reliability when lateral branches are neglected in the geometry reconstruction from biomedical images. We are interested in this situation for many reasons.

Firstly, the geometry reconstruction and the related mesh formation to obtain the patient-specific computational domain may be simplified if lateral branches are not considered. Indeed, focusing just on the main vessel can in some cases facilitate the reconstruction of the surface since often lateral branches are small and difficult to recognize. For what concerns the mesh set up, avoiding small

2

angles and vessels with small radius facilitates the formation of regular triangulations.

Secondly, the presence of lateral branches poses some difficulties in the set up of fluid-structure interaction (FSI) models. Artificial sections almost orthogonal to the vessel centerline are usually kept fixed in FSI models. In the case of vascular districts with several secondary branches, the previous approach could introduce an artificial stiffening of the arterial district (see for example [5] for an application to the ascending aorta, and [36] for the thoracic aorta). Furthermore, the three-dimensional arterial wall geometry and mesh are obtained usually from extrusion of the fluid domain, since the vessel walls are not easily detected from biomedical images. Then, the presence of small bifurcation angles could lead to a failure in the structure mesh generation.

Lastly, when considering a membrane model for the deformation of the arterial walls, the main and Gaussian curvatures of the vessel surface are needed in order to feed the governing equations, see [25]. Obviously, removing lateral branches from the main vessel makes both curvatures almost constant, simplifying the application of such FSI models.

As an example among many other cases, the approach that we propose could be particularly effective to account for the presence of intercostal arteries branching from the descending thoracic aorta. Indeed, several studies have recently analyzed the effect of such arteries on wall shear stresses, by means of the classical approach where lateral branches are fully accounted in the geometrical model, see [35, 18, 19]. We will show on a simple test case that the method proposed here could provide comparable results with a simplified geometrical setting.

The outline of the work is as follows. In Sect. 2 we review the problem of the geometry reconstruction of patient specific models in haemodynamics. In Sect. 3 we describe Nitsche's method for the prescription of defective conditions, discussing the application to problems where lateral branches are neglected from the geometrical model and we address some numerical experiments to validate the method at hand. In Sect. 4 we discuss the reliability of the method when a fluid-structure interaction model with a membrane structure is considered, complementing the description of the scheme with extensive numerical results. Finally, in Sect. 5 we address some conclusions of the work.

2 Set up of patient specific geometrical models in haemodynamics

Image segmentation is the operation of partitioning an image into different specific objects. In the context of patient-specific computational fluid dynamics it provides the surface identifying the interface between blood and vessel wall and consequently the volumetric domain for the simulation itself. Crucial features of the images, typically dimensionality, spatial resolution and, given the recent technological advances in the radiological field, temporal resolution, determine

the segmentation technique to be applied and the accuracy of the results. In an ideal situation all the vessels in a specific vascular district should be reconstructed and included in the model to properly represent the in-vivo condition. In many real situations some collateral or side branches may be difficult to model due to their small caliper compared to the image resolution or to suboptimal quality of the available images. In these cases the proposed approach could be an important improvement to the simplistic solution of omitting unavailable side branches.

The aortic arch is a challenging benchmark test for haemodynamics, because of high speed flow and corresponding complex flow patterns as well as for the study of non perturbing boundary conditions for inflow and outflow artificial sections, see for instance [5, 8, 20, 21, 22, 36]. For this reason, we exploit a patient specific aortic arch model to test the validity of the present method. The package VMTK (http://www.vmtk.org) was used for the preparation of the 3D model.

An MRI scansion of the aortic arch was obtained at *Ospedale Borgo Trento* in Verona, Italy. The images were acquired with a 1.5 Tesla machine (Magnetom Simphony, Siemens Medical Systems, Erlangen, Germany) after injection of contrast agent and saved in DICOM format for subsequent processing. The following parameters were used: TE=1.6 ms, flip angle=65°, slice thickness=6 mm, field of view=400 mm, acquisition matrix =$256\times$ 256. The images were segmented by means of the segmentation tool available within VMTK based on a gradient-driven level-set approach [1]; the complete model of the aortic arch was reconstructed from the aortic root to the first portion of the descending aorta including the three main branches that originate from it: the brachiocephalic, the left common carotid and the left subclavian arteries. We depict in Figure 1 (top, left) the complete model of the aortic arch.

To provide a model of the aortic arch where side branches have been removed, two sets of the VMTK tools for editing 3D triangulated surfaces were employed: first, the branches were manually clipped from the arch; secondly the resulting holes on the arch surface were re-meshed by progressively and smoothly, i.e. following the local surface curvature, fill them in with concentric triangulated circular strips. The triangles that eventually capped the aortic arch surface were coherently marked in order to keep trace of where the removed arteries were originally positioned, see Figure 1 (right column) for a description of the model after the removal of sovra-aortic branches.

In both cases, valve leaflets opening and closing mechanisms were not taken into account, so that numerical simulations have been performed in the systolic configuration. In particular, an analytical model of the aortic valve orifice was defined as a circle of area $3.0\,cm^2$ (see Figure 1, bottom, left). Moreover, the leaflets were not drawn, since their modelization is outside of the goals of this work.

The solid model was successively turned into a volumetric mesh of linear tetrahedra in order for computational fluid-dynamics simulations to be carried
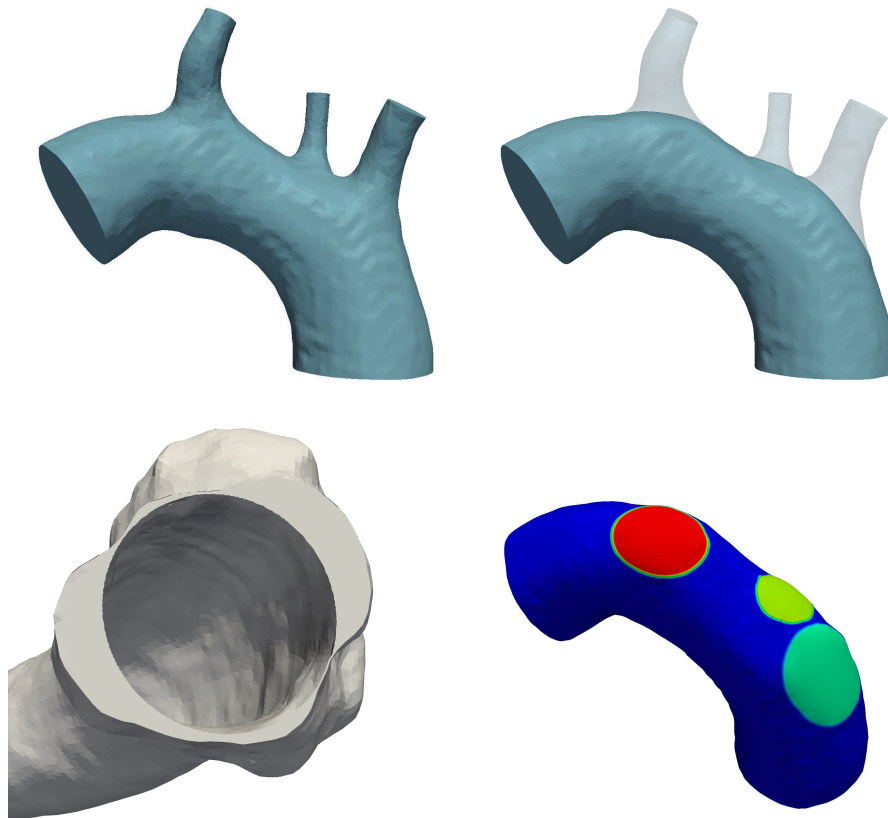
4

Figure 1: Patient specific model of the aortic arch including the brachiocephalic, the left common carotid and the left subclavian arteries (top, left), compared with the analogous model without side branches (top, right). On the bottom, a detail of the valve orifice at systole (bottom, left) and of the outflow sections reconstructed on the surface of the aortic wall in correspondence of the removed lateral branches (bottom, right).

out. We have 227858 tetrahedra for the mesh with lateral branches and 198292 tetrahedra for the mesh without lateral branches. These dimensions were reached after successive mesh refinements, with the aim of obtaining a mesh-independent numerical solution.

3 Outflow boundary conditions for lateral branches.

3.1 Steady Navier-Stokes model with rigid walls.

We assume that blood behaves as a homogeneous and Newtonian fluid [11], and that the arterial walls could be considered as rigid boundaries. Reminding that $\mathbf{u}$ denotes the blood flow velocity, p the pressure and μ the blood dynamic viscosity, we define the strain rate and the Cauchy stress tensor as follows

$$\mathbf{D}(\mathbf{u}) := \frac{1}{2}\big(\nabla\mathbf{u} + \nabla'\mathbf{u}\big), \quad \mathbf{T}(\mathbf{u}, p) := 2\mu\mathbf{D}(\mathbf{u}) - p\mathbf{I}.$$

Let Ω be a domain representative of both *full* (Ω_f) and *reduced* (Ω_r) flow domains, see Figure 1. We assume that such domains feature N outflow sections (distal artificial sections with respect to the heart) and a single inflow section (proximal to the heart). We denote by Γ_i such artificial sections, where Γ_0 corresponds to the inflow and Γ_k with $k = 1, \ldots, N$ represent the outflow sections. We denote with $\Gamma := \cup_{k=0}^{N}\Gamma_k$ the union of all artificial sections, then $\partial\Omega \setminus \Gamma$ corresponds to the arterial wall.

As previously observed, one of the main issues in computational haemodynamics consists in providing boundary conditions for the artificial sections Γ_k that separate the considered vascular district Ω from the remaining part of the arterial tree. In absence of accurate data on inflow and outflow velocity profiles, boundary conditions that minimally perturb blood flow should be applied. In particular, mean flow rate or mean pressure conditions (or equivalently mean normal stress) are often applied to computational haemodymamics studies [15, 10, 30, 31, 12, 34, 37]. A more general model consists in enforcing a linear combination of the two previous conditions [33, 5, 32]. Denoting by ρ_f the constant fluid density, by Q_k a reference flow rate, by P_k the mean stress and by R_k a constant coefficient, such condition prescribes that

$$\rho_f R_k\Big(\int_{\Gamma_k}\mathbf{u}\cdot\mathbf{n}\,ds - Q_k\Big) + \Big(\int_{\Gamma_k}\mathbf{n}'\mathbf{T}(\mathbf{u}, p)\mathbf{n}\,ds + P_k\Big) = 0. \qquad (1)$$

Previous conditions can be interpreted as *mean resistance conditions*, that prescribe a constitutive law between the blood flow rate through an artificial section Γ_k and the resistance to discharge, in the spirit of Poiseuille law for a laminar flow in a straight tube. In this case, the parameter R_k assumes the role of resistance to flow induced by the arterial tree distal to the artificial section.

We observe that boundary conditions (1) only constrain the mean value of normal velocity components and stresses. Therefore, they are not sufficient to

ensure that, combined with Navier-Stokes equations for conservation of mass and momentum, the problem is uniquely solvable. For this reason such type of conditions is often classified as being *defective*. To override this drawback, additional conditions on stresses at the artificial sections must be prescribed. More precisely, we require that the normal stress vector is constant along each artificial section Γ_k, with unknown modulus along the normal direction to the considered section, that is

$$\mathbf{T}(\mathbf{u}, p)\mathbf{n} = c_k \mathbf{n} \quad \text{on } \Gamma_k \quad \text{or equivalently}$$

$$\mathbf{n}'\mathbf{T}(\mathbf{u}, p)\mathbf{n} = c_k, \quad \mathbf{n} \times \mathbf{T}(\mathbf{u}, p)\mathbf{n} = 0 \quad \text{on } \Gamma_k,$$

for suitable constants c_k. Then, given Q_k, P_k and R_k with $k = 0, \ldots, N$, and the forcing term $\mathbf{f}$, our reference problem consists to find velocity and pressure fields $\mathbf{u}, p$ and constants c_k such that

$$\begin{cases} -\mu\nabla \cdot \left(\nabla\mathbf{u} + \nabla'\mathbf{u}\right) + \rho_f\left(\mathbf{u} \cdot \nabla\right)\mathbf{u} + \nabla p = \mathbf{f} & \text{in } \Omega, \\ \nabla \cdot \mathbf{u} = 0 & \text{in } \Omega, \\ \mathbf{u} = \mathbf{0} & \text{on } \partial\Omega \setminus \Gamma, \quad (2) \\ \rho_f R_k\left(\int_{\Gamma_k} \mathbf{u} \cdot \mathbf{n}\, ds - Q_k\right) + \left(\int_{\Gamma_k} \mathbf{n}'\mathbf{T}(\mathbf{u}, p)\mathbf{n}\, ds + P_k\right) = 0 & \text{on } \Gamma_k, \\ \mathbf{T}(\mathbf{u}, p)\mathbf{n} = c_k\mathbf{n} & \text{on } \Gamma_k. \end{cases}$$

Most often parameters R_k, P_k should be provided by suitable mathematical models for the distal arterial tree, see for instance [26]. Although the problem setting is kept general throughout this section, for the numerical investigation we restrict to flow rate boundary conditions, which correspond to (1) with $R_k \to \infty$. In particular, we assume that the entire flow division is provided in our case. More precisely, for each outflow section Γ_k with $k = 1, \ldots, N$, the flow rate Q_k is known, while the inflow flow rate is provided by enforcement of mass conservation constraint, i.e. $Q_0 = -\sum_{k=1}^N Q_k$.

Remark 1 *For the sake of completeness, we notice that it is possible to generalize defective boundary conditions to account for the angle of incidence between the main channel and the outgoing vessels. This gives rise to the following condition,*

$$\rho_f R_k\left(\int_{\Gamma_k} \mathbf{u}\, ds - \mathbf{Q}_k\right) + \left(\int_{\Gamma_k} \mathbf{T}(\mathbf{u}, p)\mathbf{n}\, ds + \mathbf{P}_k\right) = \mathbf{0},$$

where $\mathbf{Q}_k \in \mathbb{R}^3$, $\mathbf{P}_k \in \mathbb{R}^3$. By this way, the mean value of the tangential components of the velocity and of the normal stress vector are also taken into account. We refer to this condition as vector valued defective condition.

3.2 Numerical treatment of resistance boundary conditions.

Let $\mathcal{T}_h$ be a family of admissible, shape regular and quasi-uniform triangulations of Ω with characteristic mesh size h. We denote by $\mathbf{V}_h$ and Q_h respectively, the

selected finite element spaces for velocity and pressure approximation, which will be specified later on. For the forthcoming method the choice of such spaces is independent of the definition of boundary conditions on artificial sections. Then, the main difficulty for the approximation of problem (2) in the framework of the finite element method consists in embedding resistance boundary conditions into the scheme. Our approach is based on the reinterpretation of (1) as an averaged Robin-type (or mixed type) boundary condition, which consists in the following rearrangement,

$$\int_{\Gamma_k} \mathbf{n}' \mathbf{T}(\mathbf{u}, p) \mathbf{n}\, ds = \mathcal{G}_k - \mu \mathcal{R}_k \int_{\Gamma_k} \mathbf{u} \cdot \mathbf{n}\, ds \tag{3}$$

$$\text{with} \quad \mathcal{R}_k := \frac{\rho_f R_k}{\mu}, \quad \mathcal{G}_k := \mu \mathcal{R}_k Q_k - P_k.$$

We aim to develop a general approximation scheme capable to handle the entire range of admissible Robin coefficients $\mathcal{R}_k$, from the case of mean stress conditions, corresponding to the limit $\mathcal{R}_k \to 0$, to the flow rate conditions obtained when $\mathcal{R}_k \to \infty$. Furthermore, the selected approximation scheme should be robust, namely the stability of the scheme must not depend on $\mathcal{R}_k$. In particular, by multiplying the momentum equation by a test function $\mathbf{v}$ and apply Green's formula to the viscous term and to the pressure, and by exploiting the fact that $\mathbf{T}(\mathbf{u}, p)\mathbf{n}$ is constant and aligned with the normal direction on each section Γ_k, we obtain,

$$\big(2\mu \mathbf{D}(\mathbf{u}), \mathbf{D}(\mathbf{v})\big)_\Omega + \big(\rho_f(\mathbf{u} \cdot \nabla)\mathbf{u}, \mathbf{v}\big)_\Omega - \big(p, \nabla \cdot \mathbf{v}\big)_\Omega$$
$$- \big(\mathbf{T}(\mathbf{u}, p)\mathbf{n}, \mathbf{v}\big)_{\partial\Omega \setminus \Gamma} - \sum_k \big\langle \mathbf{n}' \mathbf{T}(\mathbf{u}, p)\mathbf{n}, \mathbf{v} \cdot \mathbf{n} \big\rangle_{\Gamma_k} = \big(\mathbf{f}, \mathbf{v}\big)_\Omega \tag{4}$$

where $(\cdot, \cdot)_\Omega$ is the L^2 inner product and $\langle \cdot, \cdot \rangle_\Sigma$ denotes the following symmetric positive semidefinite bilinear form [37],

$$\langle u, v \rangle_\Sigma := \frac{1}{|\Sigma|} \int_\Sigma u\, ds \int_\Sigma v\, ds.$$

We observe that equation (3) could now be naturally enforced into (4), by substitution into the last term on the left hand side, namely $\langle \mathbf{n}' \mathbf{T}(\mathbf{u}, p)\mathbf{n}, \mathbf{v} \cdot \mathbf{n} \rangle_{\Gamma_k}$. However, to improve the generality and the robustness of the resulting scheme, we opt for a technique recently proposed in [17] to weakly enforce Robin conditions for the Laplacian, then extended in [32, 37] to the defective-Stokes case. This approach is based on suitable linear combinations of (3) and (4), and contrarily to the approach based on simple substitution, it has the advantage to be applicable to the entire range of parameters $\mathcal{R}_k$, including $\mathcal{R}_k \to \infty$ that corresponds to the pure flow rate boundary conditions.

Given a penalty parameter γ to be specified later on, by following [32] we obtain the governing equations for the desired finite element approximation of

problem (2), which consists to find $\mathbf{u}_h \in \mathbf{V}_h$ and $p_h \in Q_h$ such that

$$\begin{cases} a_{\mathcal{R},h}(\mathbf{u}_h; \mathbf{u}_h, \mathbf{v}_h) + b_{\mathcal{R},h}(p_h, \mathbf{v}_h) = F_{\mathcal{R},h}(\mathbf{v}_h) & \forall \mathbf{v}_h \in \mathbf{V}_h \\ b_{\mathcal{R},h}(q_h, \mathbf{u}_h) + c_{\mathcal{R},h}(p_h, q_h) = G_{\mathcal{R},h}(q_h) & \forall q_h \in Q_h \end{cases} \tag{5}$$

where $a_{\mathcal{R},h}(\cdot, \cdot)$, $b_{\mathcal{R},h}(\cdot, \cdot)$, $c_{\mathcal{R},h}(\cdot, \cdot)$ are defined as follows,

$$a_{\mathcal{R},h}(\mathbf{w}; \mathbf{u}, \mathbf{v}) := \big(2\mu \mathbf{D}(\mathbf{u}), \mathbf{D}(\mathbf{v})\big)_\Omega + \big(\rho_f(\mathbf{w} \cdot \nabla)\mathbf{u}, \mathbf{v}\big)_\Omega + \sum_k \frac{\mu \mathcal{R}_k}{1 + \gamma \mathcal{R}_k h} \left\langle \mathbf{u} \cdot \mathbf{n}, \mathbf{v} \cdot \mathbf{n} \right\rangle_{\Gamma_k}$$

$$- \sum_k \frac{\gamma \mathcal{R}_k h}{1 + \gamma \mathcal{R}_k h} \left[\left\langle 2\mu \mathbf{n}' \mathbf{D}(\mathbf{u})\mathbf{n}, \mathbf{v} \cdot \mathbf{n} \right\rangle_{\Gamma_k} + \left\langle 2\mu \mathbf{n}' \mathbf{D}(\mathbf{v})\mathbf{n}, \mathbf{u} \cdot \mathbf{n} \right\rangle_{\Gamma_k} \right]$$

$$- \sum_k \frac{\gamma}{1 + \gamma \mathcal{R}_k h} \frac{h}{\mu} \left\langle 2\mu \mathbf{n}' \mathbf{D}(\mathbf{u})\mathbf{n}, 2\mu \mathbf{n}' \mathbf{D}(\mathbf{v})\mathbf{n} \right\rangle_{\Gamma_k}$$

$$b_{\mathcal{R},h}(q, \mathbf{v}) := -\big(p, \nabla \cdot \mathbf{v}\big)_\Omega + \sum_k \frac{\gamma \mathcal{R}_k h}{1 + \gamma \mathcal{R}_k h} \left\langle q, \mathbf{v} \cdot \mathbf{n} \right\rangle_{\Gamma_k}$$

$$+ \sum_k \frac{\gamma}{1 + \gamma \mathcal{R}_k h} \frac{h}{\mu} \left\langle q, 2\mu \mathbf{n}' \mathbf{D}(\mathbf{v})\mathbf{n} \right\rangle_{\Gamma_k}$$

$$c_{\mathcal{R},h}(p, q) := -\sum_k \frac{\gamma}{1 + \gamma \mathcal{R}_k h} \frac{h}{\mu} \left\langle p, q \right\rangle_{\Gamma_k}$$

where, to simplify the description of the scheme, we have assumed that the finite element space conforms with no-slip boundary conditions on $\partial\Omega \setminus \Gamma$, i.e. $\mathbf{V}_h \in \mathbf{H}^1_{\partial\Omega \setminus \Gamma}(\Omega)$ so that $\big(\mathbf{T}(\mathbf{u}, p)\mathbf{n}, \mathbf{v}\big)_{\partial\Omega \setminus \Gamma} = 0$. However, in the forthcoming numerical experiments we will apply Nitsche's type approximation of no-slip conditions at the interface with rigid walls. The right hand side terms in (5) are,

$$F_{\mathcal{R},h}(\mathbf{v}) := \big(\mathbf{f}, \mathbf{v}\big)_\Omega - \sum_k \frac{1}{1 + \gamma \mathcal{R}_k h} \frac{1}{|\Gamma_k|} \left\langle \mathcal{G}_k, \mathbf{v} \cdot \mathbf{n} \right\rangle_{\Gamma_k} - \sum_k \frac{\gamma}{1 + \gamma \mathcal{R}_k h} \frac{h}{\mu} \frac{1}{|\Gamma_k|} \left\langle \mathcal{G}_k, 2\mu \mathbf{n}' \mathbf{D}(\mathbf{v})\mathbf{n} \right\rangle_{\Gamma_k},$$

$$G_{\mathcal{R},h}(q) := \sum_k \frac{\gamma}{1 + \gamma \mathcal{R}_k h} \frac{h}{\mu} \frac{1}{|\Gamma_k|} \left\langle \mathcal{G}_k, q \right\rangle_{\Gamma_k}.$$

In previous definitions of bilinear and linear forms, the suffix $\mathcal{R}$ stands for the collection of values $[\mathcal{R}_0, \ldots, \mathcal{R}_N]$, highlighting the dependence of the forms on the value of the resistances.

It has been proved in [32] that the linearized version of problem (5) (that is the Oseen problem) is well posed and robust provided that the stability parameter γ is smaller than a given threshold.

3.3 Stabilization technique for inflow sections and flow reversal.

In the seminal work [15] Heywood, Rannacher and Turek observed that, in contrast to Dirichlet boundary conditions, the application of mean pressure or

mean flow rate conditions results in a difficulty in estimating the energy balance across artificial sections. A similar issue consists on the simulation divergence due to flow reversal at outflow boundaries as addressed in [5] and extensively analyzed in [8], where different stabilization approaches are compared.

In our view, the theory developed in [15] already sheds light on an efficient and sound technique to override this drawback. In particular, owing to the identity $\frac{1}{2}\nabla|\mathbf{u}|^2 = \mathbf{u}(\nabla\mathbf{u})^T$, the convection term $\left(\rho_f(\mathbf{u}\cdot\nabla)\mathbf{u}, \mathbf{v}\right)_\Omega$ can be replaced with its symmetric form

$$\left(\rho_f(\mathbf{u}\cdot\nabla)\mathbf{u}, \mathbf{v}\right)_\Omega - \left(\rho_f(\mathbf{v}\cdot\nabla)\mathbf{u}, \mathbf{u}\right)_\Omega + \frac{1}{2}\left(\rho_f\nabla|\mathbf{u}|^2, \mathbf{v}\right)_\Omega, \tag{6}$$

where the kinetic energy $\frac{1}{2}\rho_f|\mathbf{u}|^2$ can be combined with the hydrostatic pressure to give the total pressure $P := p + \frac{1}{2}\rho_f|\mathbf{u}|^2$. Then, reformulating the resistance conditions in terms of total pressure and resorting to the symmetrization of the convective term could restore the control on kinetic energy balance. However, it has been observed that such technique provides unsatisfactory results of artificial outflow boundaries, see for instance Figure 8 in [15], which is the most significant case for us. In alternative, we consider the introduction of a stabilization term to restore control on the kinetic energy at inflow and outflow sections. Such technique, originally proposed in [5], can be reinterpreted in the present framework. Setting $\mathbf{v} = \mathbf{u}$ into (6) and applying integration by parts we easily conclude that

$$\left(\rho_f(\mathbf{u}\cdot\nabla)\mathbf{u}, \mathbf{u}\right)_\Omega = \frac{\rho_f}{2}\int_{\partial\Omega} \mathbf{u}\cdot\mathbf{n}|\mathbf{u}|^2\, ds.$$

It is straightforward to see that neither resistance nor flow rate conditions allow to control such residual boundary terms. This task is achieved by the introduction into the momentum bilinear form $a_{\mathcal{R},h}(\mathbf{w};\mathbf{u},\mathbf{v})$ of the following stabilization term

$$s_k(\mathbf{w};\mathbf{u},\mathbf{v}) := \frac{\rho_f}{2}\int_{\Gamma_k}\left(|\mathbf{w}\cdot\mathbf{n}| - \mathbf{w}\cdot\mathbf{n}\right)\mathbf{u}\cdot\mathbf{v}\, ds, \tag{7}$$

complemented by the right hand side $s_k(\mathbf{w};\mathbf{U}_k,\mathbf{v})$, being $\mathbf{U}_k$ a given velocity profile. In particular, for outflow sections we consider $\mathbf{U}_k = \mathbf{0}$ with $k = 1, 2, 3, \ldots$, while for the inflow section Γ_0 we propose to apply a flat velocity profile $\mathbf{U}_0 = (Q_0/|\Gamma_0|)\mathbf{n}$.

We immediately verify that, if no-slip conditions on the arterial wall are embedded into the solution search space, the stabilization term restores the positivity of the convective terms at the boundaries,

$$\left(\rho_f(\mathbf{u}\cdot\nabla)\mathbf{u}, \mathbf{u}\right)_\Omega + \sum_k s_k(\mathbf{u};\mathbf{u},\mathbf{u}) = \frac{\rho_f}{2}\int_\Gamma |\mathbf{u}\cdot\mathbf{n}||\mathbf{u}|^2\, ds \geq 0.$$

Unfortunately, the introduction of this new term violates the strong consistency of the scheme (5) with the governing equations (2). Then, a natural question to address concerns the characterization of the new governing equations after the

10

introduction of the stabilization term, with special attention to the boundary conditions.

In particular, the term $s_k(\mathbf{w}; \mathbf{u} - \mathbf{U}_k, \mathbf{v})$ can be interpreted in multiple ways. On the one hand, it can be seen as a penalization term corresponding to the weak enforcement of the pointwise conditions $\mathbf{u} = \mathbf{U}_k$ on Γ_k. In this case, the penalty parameter directly depends on the negative part in the inflow / outflow convective velocity, namely $\frac{1}{2}(|\mathbf{w} \cdot \mathbf{n}| - \mathbf{w} \cdot \mathbf{n})$. By this way, the stabilization is active only for the part of the boundary where the flow is entering the domain.

On the other hand, as previously remarked in [5, 8], the introduction of $s_k(\mathbf{w}; \mathbf{u}, \mathbf{v})$ can be compared with the aforementioned application of total pressure to resistance boundary conditions. Indeed, the stabilization technique corresponds to replacing the constraint $\mathbf{T}(\mathbf{u}, p)\mathbf{n} = c_k\mathbf{n}$ with $\mathbf{T}(\mathbf{u}, p)\mathbf{n} + \frac{1}{2}(|\mathbf{u} \cdot \mathbf{n}| - \mathbf{u} \cdot \mathbf{n})\mathbf{u} = c_k\mathbf{n}$. Then, equation (3) becomes

$$\int_{\Gamma_k} \mathbf{T}(\mathbf{u}, p)\mathbf{n}\, ds = \mathcal{G}_k - \mu\mathcal{R}_k\left(\int_{\Gamma_k} \mathbf{u} \cdot \mathbf{n}\right)\mathbf{n}\, ds - \frac{1}{2}\int_{\Gamma_k}(|\mathbf{u}\cdot\mathbf{n}| - \mathbf{u}\cdot\mathbf{n})\mathbf{u}\, ds \text{ on } \Gamma_k. \quad (8)$$

Then, replacing (8) into the weak form of the Navier-Stokes momentum equation, the additional term $\sum_k \frac{1}{2}\big((|\mathbf{u} \cdot \mathbf{n}| - \mathbf{u} \cdot \mathbf{n})\mathbf{u}, \mathbf{v}\big)_{\Gamma_k}$ appears, which is exactly $\sum_k s_k(\mathbf{u}; \mathbf{u}, \mathbf{v})$. This shows that the proposed stabilization technique corresponds to modify the traction force at the artificial sections where flow reversal takes place.

3.4 Numerical solver

Problem (5) does not yet correspond to an uniquely solvable discrete linear problem and several steps are necessary to cast it into such a framework.

As previously remarked, formulation (5) does not set any specific constraints for the definition of the finite element spaces $\mathbf{V}_h, Q_h$. To obtain an easily implementable scheme, we opt for the equal order affine approximation for velocity and pressure fields. It is well known that such choice violates the *inf-sup* stability condition for mixed problems such as (5). To restore stability of the discrete problem we resort to the so called Brezzi-Pitkaranta stabilized formulation (we refer the interested reader to [29] and references therein), which is based on the relaxation of the incompressibility constraint by means of the introduction of the following additional term

$$d_h(p_h, q_h) := \frac{\gamma_p h^2}{\mu}\int_\Omega \nabla p_h \cdot \nabla q_h$$

into the continuity equation of (5), which becomes

$$b_{\mathcal{R},h}(q_h, \mathbf{u}_h) + c_{\mathcal{R},h}^{stab}(p_h, q_h) = G_{\mathcal{R},h}(q_h), \ \forall q_h \in Q_h,$$

where we have set $c_{\mathcal{R},h}^{stab}(\cdot, \cdot) := c_{\mathcal{R},h}(\cdot, \cdot) + d_h(\cdot, \cdot)$. The parameter γ_p is chosen to guarantee stability and appropriate conditioning of the discrete system of equations.

Another source of instability comes from the fact that the momentum equation for blood flow in large or medium sized arteries is usually convection dominated. To treat the lack of stability of the finite element method in these conditions, we apply the classical streamline upwind method which consist to modify the bilinear form $a_{\mathcal{R},h}(\cdot,\cdot)$ as follows,

$$a_{\mathcal{R},h}^{stab}(\mathbf{w};\mathbf{u},\mathbf{v}) := a_{\mathcal{R},h}(\mathbf{w};\mathbf{u},\mathbf{v}) + \frac{\gamma_v \rho_f h^2}{\mu} \int_\Omega ((\mathbf{w}\cdot\nabla)\,\mathbf{u})\cdot((\mathbf{w}\cdot\nabla)\,\mathbf{v}),$$

where γ_v is a parameter to be suitably chosen.

We finally observe that for the forthcoming numerical investigations we will consider the particular case obtained by taking $R_k \to \infty$, corresponding to mean flow rate conditions on each artificial section Γ_k. Owing to the generality and the robustness of the method, the limit cases $R_k \to 0$ or $R_k \to \infty$ can be straightforwardly obtained by restriction of the bilinear forms, indeed all the scaling expressions depending on R_k remain bounded for any value of the parameter. For the sake of clarity, we report here the problem with flow rate conditions, which takes the form (we omit the suffix $\mathcal{R}$ to identify this case, that is $\mathcal{R}_k \to \infty$, $k = 0,\ldots,N$)

$$\begin{cases} a_h^{stab}(\mathbf{u}_h;\mathbf{u}_h,\mathbf{v}_h) + b_h(p_h,\mathbf{v}_h) = F_h(\mathbf{v}_h) & \forall \mathbf{v}_h \in \mathbf{V}_h, \\ b_h(q_h,\mathbf{u}_h) + c_h^{stab}(p_h,q_h) = G_h(q_h) & \forall q_h \in Q_h, \end{cases} \qquad (9)$$

with

$$a_h^{stab}(\mathbf{w};\mathbf{u},\mathbf{v}) := \left(2\mu\mathbf{D}(\mathbf{u}),\mathbf{D}(\mathbf{v})\right)_\Omega + \left(\rho_f(\mathbf{w}\cdot\nabla)\mathbf{u},\mathbf{v}\right)_\Omega + \frac{\gamma_v \rho_f h^2}{\mu}\left((\mathbf{w}\cdot\nabla)\mathbf{u},(\mathbf{w}\cdot\nabla)\mathbf{v}\right)_\Omega$$
$$+ \sum_k \frac{\mu}{\gamma h}\langle \mathbf{u}\cdot\mathbf{n},\mathbf{v}\cdot\mathbf{n}\rangle_{\Gamma_k} - \sum_k \left[\langle 2\mu\mathbf{n}'\mathbf{D}(\mathbf{u})\mathbf{n},\mathbf{v}\cdot\mathbf{n}\rangle_{\Gamma_k} + \langle 2\mu\mathbf{n}'\mathbf{D}(\mathbf{v})\mathbf{n},\mathbf{u}\cdot\mathbf{n}\rangle_{\Gamma_k}\right],$$

$$b_h(q,\mathbf{v}) := -\left(p,\nabla\cdot\mathbf{v}\right)_\Omega + \sum_k \langle q,\mathbf{v}\cdot\mathbf{n}\rangle_{\Gamma_k},$$

$$c_h^{stab}(p,q) := \frac{\gamma_p h^2}{\mu}\left(\nabla p_h,\nabla q_h\right)_\Omega,$$

$$F_h(\mathbf{v}) := \left(\mathbf{f},\mathbf{v}\right)_\Omega - \langle \rho_f Q_k,\mathbf{v}\cdot\mathbf{n}\rangle_{\Gamma_k} - \langle \rho_f Q_k,2\mu\mathbf{n}'\mathbf{D}(\mathbf{v})\mathbf{n}\rangle_{\Gamma_k},$$

$$G_h(q) := \langle \rho_f Q_k,q\rangle_{\Gamma_k}.$$

$$(10)$$

We observe that the momentum equation of (9) is nonlinear because of the convective term. For simplicity, we apply dumped Picard (or fixed point) iterations to linearize it. More precisely, we replace (9) with the following sequence of problems. Given $\mathbf{u}_h^0$, for $k = 1,2,\ldots$ aim to find $\mathbf{u}_h^k \in \mathbf{V}_h$ and $p_h^k \in Q_h$ such that

$$\begin{cases} \sigma\left(\mathbf{u}_h^k - \mathbf{u}_h^{k-1},\mathbf{v}_h\right)_\Omega + a_h^{stab}(\mathbf{u}_h^{k-1};\mathbf{u}_h^k,\mathbf{v}_h) + b_h(p_h^k,\mathbf{v}_h) = F_h(\mathbf{v}_h) & \forall \mathbf{v}_h \in \mathbf{V}_h, \\ b_h(q_h,\mathbf{u}_h^k) + c_h^{stab}(p_h^k,q_h) = G_h(q_h) & \forall q_h \in Q_h, \end{cases}$$

where $\sigma > 0$ is the damping parameter to be suitably chosen for each test case.

The corresponding algebraic problem is solved by means of a pressure matrix method, which consists in the elimination of the velocity vector unknowns and the solution of the pressure Schur complement matrix. Since such system is usually ill conditioned (see for instance [29]) especially when the velocity mass matrix appears in the discrete momentum equation, the Cahouet-Chabard preconditioner has been applied to speed up GMRES iterations. We have applied such solver, implemented in the finite element library Freefem++ (see `http://www.freefem.org/ff++/`) for the approximation of the test cases addressed in the forthcoming sections.

3.5 Numerical results

The aim of this section is to validate (9) for the approximation of outflow conditions at the intersection with lateral branches. We consider two test cases, an idealized model addressed in [18] and a realistic aortic arch. Since we focus on haemodynamics applications, pressure, flow profiles and wall shear stresses (WSS) will be analyzed.

In all the numerical tests of this section and of Section 4 we have used the following values for parameters: $\gamma = 10^{-4}$, $\rho_f = 1.0\,g/cm^3$, $\mu = 0.035\,Poise$, $R_k = \mathcal{R}_k = \infty$, $\forall k$, $\gamma_p = 5 \times 10^{-4}$, $\gamma_v = 5 \times 10^{-2}$.

3.5.1 Application to an idealized model of lateral branch

The present test case has been proposed in [18] to study the effect of small lateral side branches, such as intercostal arteries, on the shear stress patterns at the wall of large arteries, such as the descending thoracic aorta.

Following [18] we consider the domain depicted in Figure 2 (top), where the main box measures $1 \times 26 \times 0.5$ cm, being (x, y, z) the lateral, longitudinal and vertical directions, respectively, and the side branch is modeled as a cylindrical segment 0.1 cm wide. The visualized computational mesh consists on 31778 tetrahedral elements.

The bulk flow is oriented form left to right, driven by a steady semi-parabolic inflow profile $u_x = 0, u_y(z) = \frac{3}{2}U(1 - (z/0.5)^2), u_z = 0$. The upper surface of the main channel corresponds to a no-slip boundary, where the velocity is fixed to zero, while on the lateral sides of the box we set homogeneous Neumann conditions. The inflow flow rate Q_0 is computed according to the inflow profile, while the lateral branch flow rate is set to $Q_1 = 0.0079\,Q_0$. The flow rate at the main outflow section on the right hand side of the box, denoted with Q_2, is set to satisfy mass conservation. The profile modulus U is chosen to make sure that the flow Reynolds number is equal to 250, which corresponds to test case (a) of Figure 2 in [18], in order to allow for a visual comparison with present results.

As depicted in Figure 2 (middle row) we consider two configurations. A full model where the lateral branch is accounted (on the left) and a simplified model

where the flow rate Q_1 is weakly enforced at the intersection of the lateral branch with the main branch (on the right). As a preliminary validation, we observe the flow profiles at the bifurcation of the side branch are rather similar.

A more significant validation is achieved in Figure 2 (bottom row) by comparing the WSS patterns on the surface of the main vessel, in the neighborhood of the side branch. In particular, we report here the modulus of the WSS vector, normalized with respect to the WSS at the inflow of the main channel. Again, the agreement between the full model and the incomplete one is satisfactory. We observe that the WSS pattern is also significantly similar to the one reported in Figure 2(a) of [18], for the full geometrical model and equivalent flow conditions.

3.5.2 Application to an aortic arch model

In this test case we consider the full aortic arch model described in Section 2, together with the variant where the ascending branches have been omitted.

For simplicity, we consider steady flow conditions, where the inflow rate Q_0 is set to 80 cm^3 s^{-1}, corresponding to the mean value over a heart beat. Concerning the outflow, the flow division between the brachiocephalic, left common carotid and left subclavian arteries is kept constant to the values $Q_1 = 5\%$, $Q_2 = 5\%$, $Q_3 = 7\%$ of the inflow Q_0, respectively, which corresponds to realistic haemodynamic conditions. In the full model such flow rates are weakly enforced on the distal section of each branch, while for the reduced model equivalent boundary conditions are set on the outflow sections Γ_k, with $k = 1, 2, 3$, laying on the reconstructed surface of the main branch, as depicted in Figure 1 (bottom, right). According to these conditions, the inflow and outflow velocity profiles were not a priori enforced, but determined by the flow governing equations to satisfy the constraints of given flow rate and constant stresses.

In Figure 3 we compare the pressure fields (top), velocity profiles (middle) and WSS distributions (bottom) for the full and the incomplete model (left and right columns respectively). Again, the results for the two models remarkably agree. This confirms the effectiveness of the defective flow rate conditions to correctly capture the outflow profile, even though the geometrical features of the lateral branches are omitted.

4 Fluid structure interaction with outflow boundary conditions on lateral branches

4.1 Preliminaries

We notice that now the domain moves in time, so that we distinguish between the *current* configuration Ω^t, which changes in time, and the *reference* configuration Ω^0, which corresponds to the initial fixed geometry. When the fluid domain is moving, a classical Eulerian approach is not suitable for writing the fluid equations since one would like to follow the movement of the fluid-structure
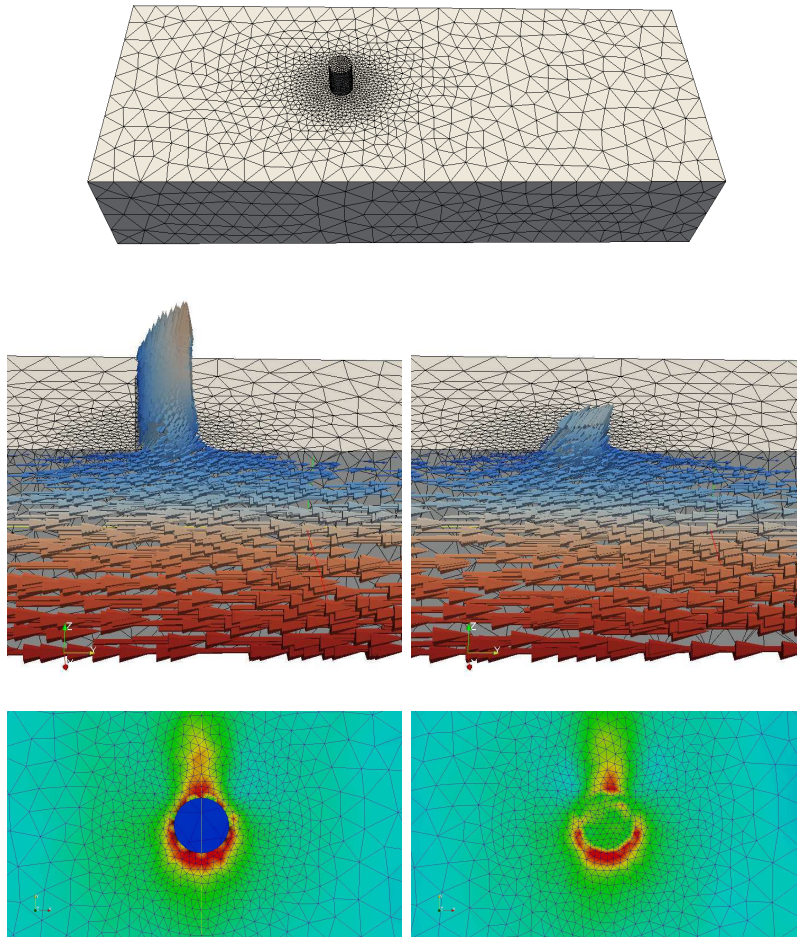
14

Figure 2: Details of the idealized model of lateral branch (as in [18]). Geometry (top), lateral outflow velocity profiles (middle) and corresponding WSS (bottom) are depicted. For the last two rows, we report the case where the lateral side branch is accounted (left) as well as the one without it (right).
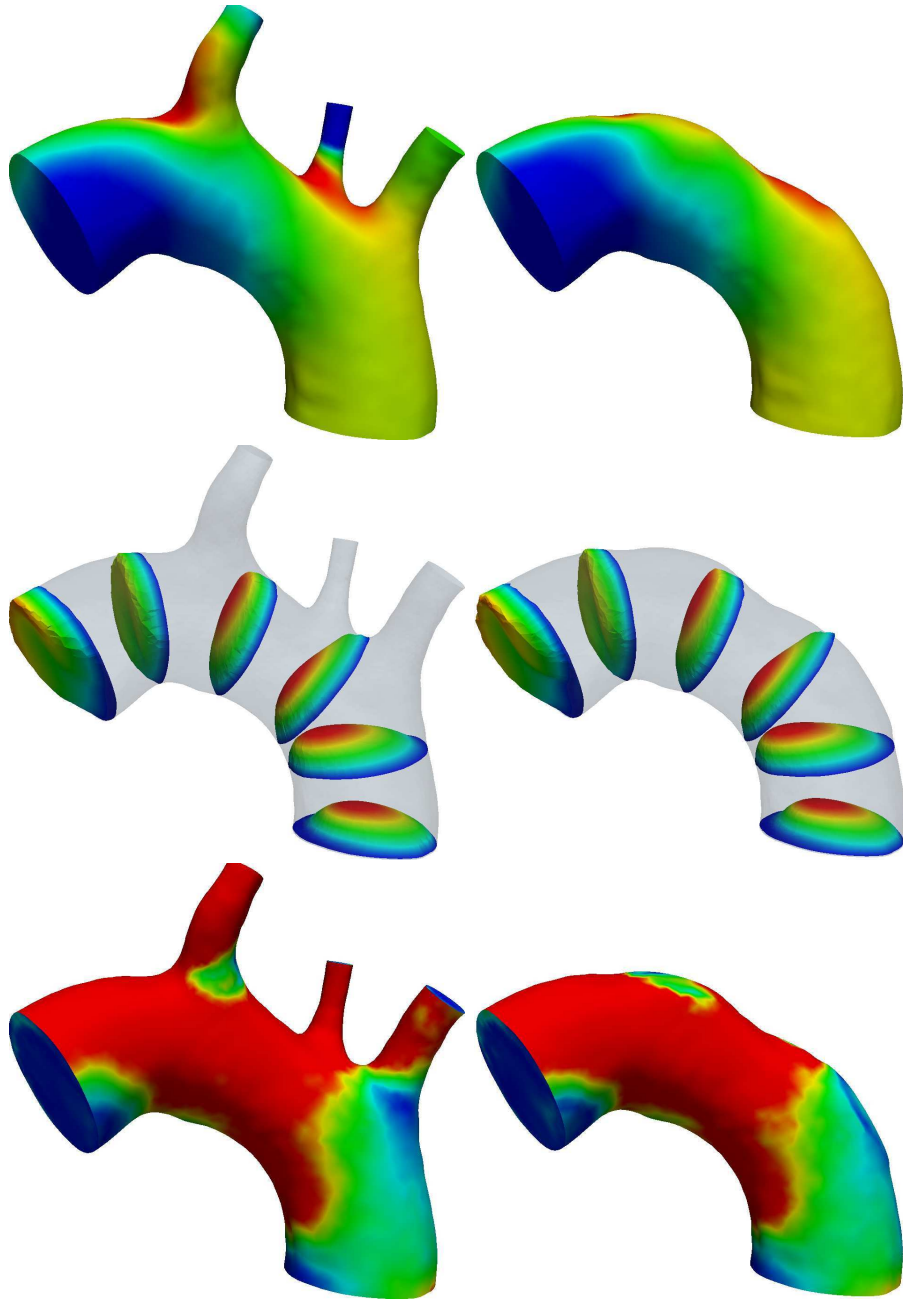
Figure 3: From top to bottom we depict the pressure fields, velocity profiles and WSS distributions for the full and the incomplete aortic arch models, corresponding to left and right columns respectively.

(FS) interface. On the other hand, a pure Lagrangian framework would deform the fluid domain also at the artificial sections. Therefore, the fluid equations are written in a hybrid configuration, namely the *Arbitrary Lagrangian-Eulerian* (ALE) framework (see e.g. [16, 7]). To this aim we consider the ALE map $\mathcal{A}$. A classical choice in haemodynamic applications to define the ALE map is to consider a harmonic extension of the structure displacement at the FS interface $\Sigma^t := \partial\Omega^t \setminus \Gamma^t$ in the reference domain (see, e.g., [6]), and to fix the artificial section (at least) in the normal direction. For any function v living in the current configuration, we denote by $\widehat{v} := v \circ \mathcal{A}$ its counterpart in the reference configuration.

As pointed out previously, with current imaging devices displacement is mainly retrieved on the interface between fluid and structure, so that extrusion of fluid mesh is needed to obtain structure meshes. However, the thickness of the vessel is not acquired by these devices, so that *a priori* assumptions on it are mandatory. Furthermore, the vascular wall is usually thinner than the lumen. For these reasons, in order to reduce the computational time, we consider here the vascular wall as a thin membrane. In particular, the membrane law considered in this work is the simple *interial-algebraic* law [25]

$$\rho_s h_s \frac{\partial^2 \widehat{\eta}}{\partial t^2} + \widehat{\beta} h_s \widehat{\eta} = \widehat{f}_s \qquad \text{in } \Sigma^0, \tag{11}$$

where ρ_s is the structure density, $\beta = \frac{E}{1-\nu^2}\beta*$ with $\beta^* = (4\rho_1^2 - 2(1-\nu)\rho_2)$, where ρ_1 and ρ_2 are the *mean* and the *Gaussian curvature*, h_s is the thickness of the membrane, E the Young modulus and ν the Poisson ratio. Here, η is the structure displacement in the normal direction with respect to Σ^0, and f_s the external forces. We observe that we have written the structure equation as usual in the Lagrangian framework.

As it emerges from the membrane law (11), the knowledge of the curvature of the FS interface is mandatory in order to write the structure problem, and consequently also the FS coupled problem, as it will be clear from the next subsection. The cut of lateral branches provides a computational domain with almost constant curvatures. As an example, in Figure 4 we depict the value of β (which depends on curvatures) for the computational domains considered in this work. We observe that by cutting the lateral branches the value of β is almost constant, while viceversa in the original domain it features values in the range $[0, 100]$. Since the case with uniform parameters leads to a better conditioned system, the case without branches is preferable for the numerical simulations. This provides another motivation for cutting lateral branches in the computational setting of cardiovascular applications.

4.2 Coupled formulation

The numerical solution of the FSI problem features two major difficulties: the *treatment of the interface position*, which is an unknown of the problem, and the
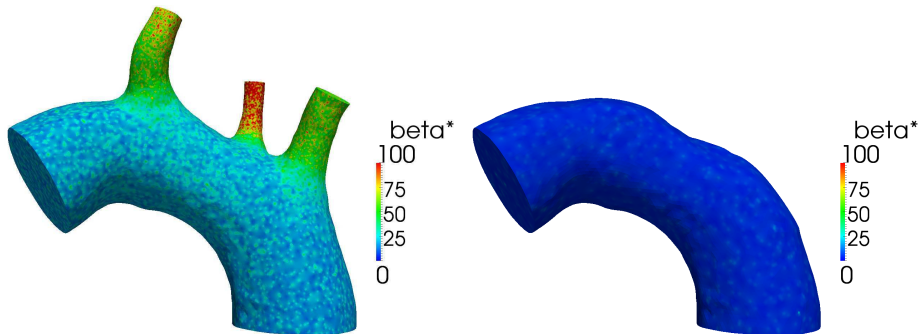
Figure 4: Magnitude of $\beta^* = (4\rho_1^2 - 2(1 - \nu)\rho_2)$, ρ_1, ρ_2 being the mean and Gaussian curvature respectively, in the case with (left) and without (right) lateral branches.

prescription of the continuity interface conditions, namely continuity of velocities and normal stresses, which reads as follows [11]

$$\begin{cases} \mathbf{u} \cdot \mathbf{n} = \eta & \text{on } \Sigma^t, \\ \mathbf{T}(\mathbf{u}, p)\mathbf{n} \cdot \mathbf{n} = -f_s & \text{on } \Sigma^t. \end{cases} \tag{12}$$

In the tangential direction, there is no coupling, so that we have to prescribe further conditions, namely either $\mathbf{u} \times \mathbf{n} = \mathbf{0}$ or $\mathbf{T}\,\mathbf{n} \times \mathbf{n} = \mathbf{0}$.

For the prescription of (12) two strategies have been proposed and widely studied in the literature, namely the *partitioned* and the *monolithic* approaches. In the first case, one solves the fluid and structure subproblems in an iterative framework, until fulfillment of the interface continuity conditions (see, e.g., [28, 6, 2]. Here, however, we consider the second strategy, based on building the whole FSI matrix, and then by solving it with an efficient method [14, 4, 13]. In this way the interface continuity conditions are automatically satisfied. The drawback of this approach is the non-modularity, in the sense that an *ad hoc* code has to be implemented, without any possibility to exploit existing fluid and structure solvers. However, here we consider the monolithic strategy introduced in [25] in the case of a membrane structure, which requires just the solution of the fluid subproblem. In particular, the structure subproblem is "embedded" into the fluid one leading to a Robin boundary condition for the fluid at the FS interface.

Concerning the treatment of the interface position, we consider here an *explicit treatment* as proposed in [9, 3], based on a suitable extrapolation of the interface position from previous time steps. Recently, in [24] it has been highlighted the effectiveness and accuracy of this treatment for haemodynamics applications.

Moreover, in order to obtain physical solutions, one has to deal with another difficulty, namely the formation of spurious pressure reflections at the outlets,

where non ad-hoc boundary conditions are prescribed. To this aim, we consider the following absorbing boundary condition at a generic outlet, introduced in [25] and obtained by a 1D reduced model,

$$\mathbf{T}(\mathbf{u}, p)\mathbf{n} \cdot \mathbf{n} = \beta \left(\left(\frac{Q_{out}}{4\chi A_{out}} + (A_{out}^0)^{1/4} \right)^2 - (A_{out}^0)^{1/2} \right),$$

where $\chi := \sqrt{\frac{\beta}{2\rho_f}}$ and $Q_{out}(t)$ and $A_{out}(t)$ (with $A_{out}^0 = A_{out}(t = 0)$) are the flow rate and the area at the outlet at hand. This condition gives an implicit relation among the normal stress, the flow rate and the area at the outlet. In the numerical simulations, we will use an explicit expression of flow rate and area, by using a suitable extrapolation of previous time steps, relying to a Neumann boundary condition.

In view of writing the time discrete problem, given a quantity z, we denote with z^n its approximation at time $t^n = t_0 + n\,\Delta t$, $t^n \in [t_0, T]$, where Δt is the time discretization parameter. Moreover, we indicate with $\mathbf{w}_h$ the finite element approximation of the fluid domain velocity. Then, after time discretization (implicit Euler for the fluid with a semi-implicit treatment of the convective term, and Backward Differentiation Formulae (BDF) of first order for the structure), the FSI problem with flow rate conditions on the artificial sections reads at each time t^{n+1} as follows [25]

1. Given $\mathbf{u}_h^n$, η_h^n, η_h^{n-1}, solve the fluid problem that is to find $\mathbf{u}_h^n, p_h^n$ such that for all $\mathbf{v}_h \in \mathbf{V}_h$ and $q_h \in Q_h$ the following equations hold true

$$\begin{cases} \frac{1}{\Delta t}(\mathbf{u}_h^{n+1} - \mathbf{u}_h^n, \mathbf{v}_h)_{\Omega^n} + a_h^{stab,n}(\mathbf{u}_h^n - \mathbf{w}_h^n; \mathbf{u}_h^{n+1}, \mathbf{v}_h) + \int_{\Sigma^n} \left(\beta h_s \Delta t + \frac{\rho_s h_s}{\Delta t} \right) \mathbf{u}_h^{n+1} \cdot \mathbf{v}_h \, ds \\ \quad + b_h^n(p_h^{n+1}, \mathbf{v}_h) = F_h^n(\mathbf{v}_h) + \int_{\Sigma^n} \left(-\beta h_s \eta_h^n + \frac{\rho_s h_s}{\Delta t^2} \left(\eta_h^n - \eta_h^{n-1} \right) \right) \mathbf{n} \cdot \mathbf{v}_h \, ds \\ \quad + \int_{\Gamma_{out}^n} \beta \left(\left(\frac{Q_{out}^n}{4\chi A_{out}^n} + (A_{out}^0)^{1/4} \right)^2 - (A_{out}^0)^{1/2} \right) \mathbf{n} \cdot \mathbf{v}_h \, ds, \\ b_h^n(q_h, \mathbf{u}_h^{n+1}) + c_h^{stab,n}(p_h^{n+1}, q_h) = G_h^n(q_h). \end{cases}$$

Superscript n over bilinear forms $a_h^{stab}(\cdot, \cdot)$, $b_h(\cdot, \cdot)$ and $c_h^{stab}(\cdot, \cdot)$ and over functionals $F_h(\cdot)$ and $G_h(\cdot)$ denotes that such quantities are evaluated over Ω^n. The number of artificial sections where a flow rate is imposed are N, namely Γ_k, $k = 0, \ldots, N-1$, and we have denoted the main outflow section with Γ_{out}. The third term at the left hand side and the second term at the right hand side of the momentum equation are related to the monolithic FSI formulation and represent a Robin boundary condition at the FS interface for the fluid due to the coupling with the membrane [25]. The third term in the right hand side of the momentum equation is due to the absorbing Neumann boundary condition at the outlet Γ_{out}.

19

2. Compute the structure displacement

$$\eta_h^{n+1} = \eta_h^n + \Delta t \mathbf{u}_h^{n+1} \cdot \mathbf{n};$$

3. Compute the fluid domain displacement by solving for all $\widehat{\mathbf{z}} \in \mathbf{Z}_h \in \mathbf{H}^1(\Omega^0)$ the following harmonic extension problem

$$\left(\nabla \widehat{\mathbf{w}}_h^{n+1}, \nabla \widehat{\mathbf{z}}\right)_{\Omega^0} + \frac{1}{\gamma\, h} \left(\widehat{\mathbf{w}}_h^{n+1}, \widehat{\mathbf{z}}\right)_{\Sigma^0} - \left(\nabla \widehat{\mathbf{w}}_h^{n+1}\mathbf{n}, \widehat{\mathbf{z}}\right)_{\Sigma^0} - \left(\nabla \widehat{\mathbf{z}}\, \mathbf{n}, \widehat{\mathbf{w}}_h^{n+1}\right)_{\Sigma^0}$$

$$+ \frac{1}{\gamma\, h} \left(\widehat{\mathbf{w}}_h^{n+1} \cdot \mathbf{n}, \widehat{\mathbf{z}} \cdot \mathbf{n}\right)_{\Gamma_0^0 \cup \Gamma_{out}^0} - \left(\mathbf{n}' \nabla \widehat{\mathbf{w}}_h^{n+1}\mathbf{n}, \widehat{\mathbf{z}} \cdot \mathbf{n}\right)_{\Gamma_0^0 \cup \Gamma_{out}^0} - \left(\mathbf{n}' \nabla \widehat{\mathbf{z}}\, \mathbf{n}, \widehat{\mathbf{w}}_h^{n+1} \cdot \mathbf{n}\right)_{\Gamma_0^0 \cup \Gamma_{out}^0}$$

$$= \frac{1}{\gamma\, h} \left(\widehat{\mathbf{u}}_h^{n+1}, \widehat{\mathbf{z}}\right)_{\Sigma^0} - \left(\nabla \widehat{\mathbf{z}}\, \mathbf{n}, \widehat{\mathbf{u}}_h^{n+1}\right)_{\Sigma^0}$$

and then update the fluid domain by

$$\mathbf{x}^{n+1} = \mathbf{x}^n + \Delta t\, \widehat{\mathbf{w}}_h^{n+1},$$

where $\mathbf{x}$ are the coordinates of the fluid domain with respect to the reference configuration. We notice Nitsche's treatment of the Dirichlet boundary condition at the FS interface for the harmonic extension. This choice allows more versatility in imposing different kind of boundary condition for the tangential and the normal components, as usually happens in this problem. In particular, we observe that we fixed the inlet Γ_0 and the outlet Γ_{out} in the normal direction by imposing a homogeneous Dirichlet condition, whilst we let them free to move in the tangential direction by imposing a homogeneous Neumann condition. Finally, we observe that at sections Γ_k, $k = 1, \ldots, N - 1$, we have imposed homogeneous Neumann conditions for all the components.

We observe that due to the explicit treatment of the interface position, the solution of the FSI problem involves just one fluid problem per time step. Therefore, this method is very interesting from the point of view of the computational time.

4.3 Numerical results

We have considered the computational domain without lateral branches addressed in the rigid case (see Figure 1, right column). We have used the same parameters and flow division of the rigid case as described in Section 3.5, as well as the same solver and code as described in Section 3.4, apart from the convective term which has been treated here explicitly. Moreover, we have set $\Delta t = 2 \cdot 10^{-3}\, s$, $\rho_s = 1.1\, g/cm^3$, and we have imposed the physiological flow rate depicted in Figure 5. In favor to the stability of the numerical scheme, the values of the flow rate have been set to four time less than physiological ones.
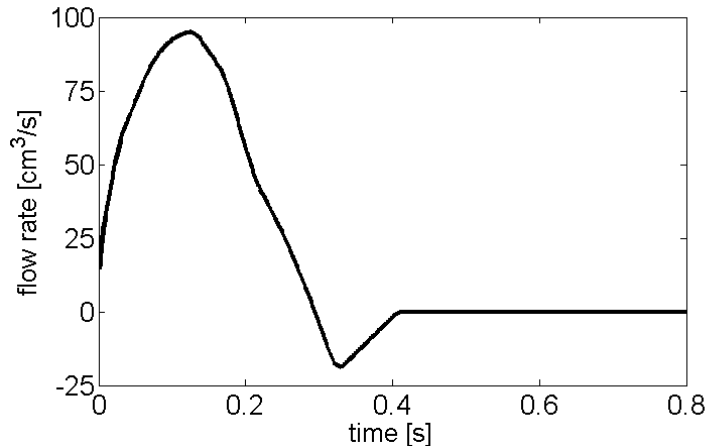
Figure 5: Flow rate prescribed at the inlet.

Therefore, the numerical results obtained by these simulations are not physiological and have to be thought as an intermediate result in view of realistic patient-specific simulations.

We have considered two sets of simulations: in the first case we have added the term (7) to the bilinear form $a_h^{stab}(\cdot,\cdot)$ $(10)_1$, whilst in the second case we have dropped it. In this way, we could evaluate the effect of (7) on the solution in terms of stabilization of flow reversals.

In Figure 6 we report the vectors of the velocity field for both cases (with and without (7)) at three different times. In particular, we consider early, peak and late systole. In the same picture the background color refers to the pressure distribution. First of all we notice the effectiveness of Nitsche's method for the prescription of the flow rate at the inlet. We observe indeed that the peak velocity at this section is moved towards the inner wall, as expected for the aortic arch. Moreover, we observe that in both cases the cut of lateral branches allows to recover a satisfying solution also in the case of a deformable vessel. In particular, the ALE map is stable and displacements of the artificial sections accounting for lateral branches are coherent to the ones of the neighboring arterial wall. This suggests that the choice of prescribing homogeneous Neumann conditions for the harmonic extension at these sections is valid in terms of stability and accuracy.

Finally, we remark the effectiveness of the stabilization induced by (7). At peak systole flow reversal does not occur at outflow sections. In this case (Figure 6, middle row) the stabilization technique does not perturb the flow. Conversely, early and late systole are characterized by transient flow patterns. During early systole flow acceleration takes place. In this case it seems unlikely to develop flow reversal, which however appears on artificial sections corresponding to lateral
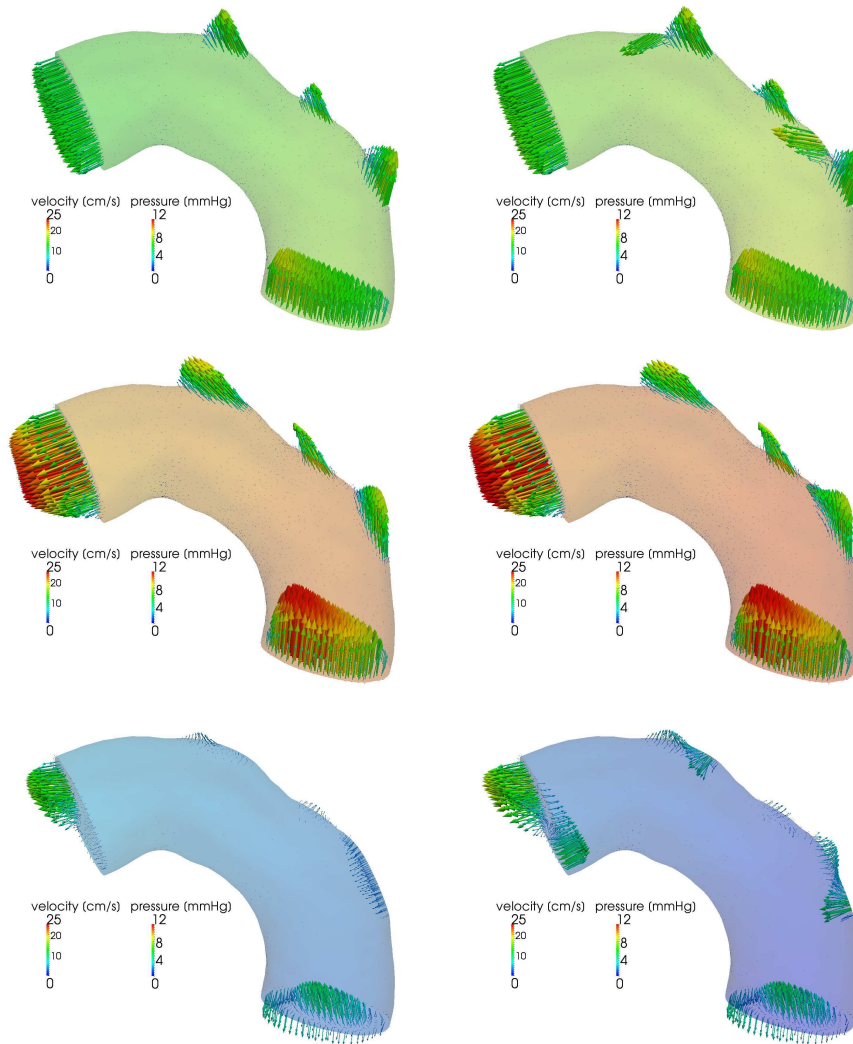
21

Figure 6: Velocity vectors on inlet and outlet sections and pressure distribution in the background for the case with (left) and without (right) stabilization term (7) - Time $t = 0.05\,s$ (top), $t = 0.11\,s$ (middle), and $t = 0.22\,s$ (bottom).

branches (Figure 6, top row). We believe that this is a spurious flow mode due to lack of pointwise control at these outflow sections. The stabilization technique is able to filter such flow conditions, restoring outward velocity field at lateral sections. The behavior at late systole is different (Figure 6, bottom row). In this case, highly decelerating flow takes place, which promotes physiological flow reversal. Indeed, it occurs at all outflow sections and we notice that the stabilization technique does not completely remove such effects, but reduces their magnitude in order to ensure stability of the discrete scheme.

5   Conclusions

In this work we have considered the problem of the prescription of average data at artificial sections in computational haemodynamics, when lateral branches are cut from the original computational domain. The interest in cutting these branches is multiple: for example, we mention a possible simplification for the geometry reconstruction and mesh generation, as well as for the treatment of the FSI problem, in particular when a membrane structure is considered (as usually done in haemodynamics). In particular, in this work we have studied the effectiveness of Nitsche's method to prescribe flow rate conditions in this context.

Firstly, we have compared the results obtained with and without lateral branches by performing steady Navier-Stokes simulation both in an idealized and in a real computational domain. In the first case, the numerical results highlighted the good accuracy of the solution obtained without lateral branches with respect to the full model also in proximity of the artificial sections. In the second case, we considered a real aortic arch as computational domain and again the results showed a good agreement among the solutions obtained in the two cases.

Secondly, we have studied the effectiveness of Nitsche's method for the prescription of the flow rate when lateral branches are cut, in the context of the FSI problem when a membrane structure is considered. Here, first of all we have noticed the significant simplification in the model due to the cut of lateral branches, since the curvature of the simplified domain is almost constant. Moreover, we have observed the effectiveness of Nitsche's method which allows to recover physiological velocity profiles without choosing them a priori. Finally, we have compared the case with and without a stabilization at the artificial sections to avoid flow reversal. These results highlighted the effectiveness of this technique, which guarantees a stable distal flow profile without affecting the solution far from the artificial sections.

Acknowledgments

References

[1] L. Antiga, M. Piccinelli, L. Botti, B. Ene-Iordache, A. Remuzzi, and D.A. Steinman. An image-based modeling framework for patient-specific computational hemodynamics. *Medical and Biological Engineering and Computing*, 46(11):1097–1112, 2008.

[2] S. Badia, F. Nobile, and C. Vergara. Fluid-structure partitioned procedures based on Robin transmission conditions. *J Comp Phys*, 227:7027–7051, 2008.

[3] S. Badia, A. Quaini, and A. Quarteroni. Splitting methods based on algebraic factorization for fluid-structure interaction. *SIAM J Sc Comp*, 30(4):1778–1805, 2008.

[4] Y. Bazilevs, V.M. Calo, Y. Zhang, and T.J.R. Hughes. Isogeometric fluid-structure interaction analysis with applications to arterial blood flow. *Computational Mechanics*, 38:310–322, 2006.

[5] Y. Bazilevs, J.R. Gohean, T.J.R. Hughes, R.D. Moser, and Y. Zhang. Patient-specific isogeometric fluid-structure interaction analysis of thoracic aortic blood flow due to implantation of the jarvik 2000 left ventricular assist device. *Computer Methods in Applied Mechanics and Engineering*, 198(45-46):3534–3550, 2009.

[6] P. Causin, J.F. Gerbeau, and F. Nobile. Added-mass effect in the design of partitioned algorithms for fluid-structure problems. *Comput Methods Appl Mech Eng*, 194(42-44):4506–4527, 2005.

[7] J. Donea. An arbitrary Lagrangian-Eulerian finite element method for transient dynamic fluid-structure interaction. *Comput Methods Appl Mech Eng*, 33:689–723, 1982.

[8] M. Esmaily Moghadam, Y. Bazilevs, T. . Hsia, I. E. Vignon-Clementel, and A. L. Marsden. A comparison of outlet boundary treatments for prevention of backflow divergence with relevance to blood flow simulations. *Computational Mechanics*, pages 1–15, 2011. Article in Press.

[9] M.A. Fernández, J.F. Gerbeau, and C. Grandmont. A projection semi-implicit scheme for the coupling of an elastic structure with an incompressible fluid. *Intern J Num Meth Eng*, 69(4):794–821, 2007.

[10] L. Formaggia, J.-F. Gerbeau, F. Nobile, and A. Quarteroni. Numerical treatment of defective boundary conditions for the Navier-Stokes equations. *SIAM J. Numer. Anal.*, 40(1):376–401 (electronic), 2002.

[11] L. Formaggia, A. Quarteroni, and A. Veneziani (Eds.). *Cardiovascular Mathematics - Modeling and simulation of the circulatory system.* Springer, 2009.

[12] L. Formaggia, A. Veneziani, and C. Vergara. A new approach to numerical solution of defective boundary value problems in incompressible fluid dynamics. *SIAM J Num Anal*, 46(6):2769–2794, 2008.

[13] M.W. Gee, U. Kuttler, and W.A. Wall. Truly monolithic algebraic multigrid for fluid-structure interaction. *Int J Num Meth Eng*, 85(8):987–1016, 2011.

[14] M. Heil. An efficient solver for the fully coupled solution of large-displacement fluid-structure interaction problems. *Comput Methods Appl Mech Eng*, 193:1–23, 2004.

[15] J.G. Heywood, R. Rannacher, and S. Turek. Artificial boundaries and flux and pressure conditions for the incompressible Navier-Stokes equations. *Internat. J. Numer. Methods Fluids*, 22(5):325–352, 1996.

[16] T. J. R. Hughes, W. K. Liu, and T. K. Zimmermann. Lagrangian-Eulerian finite element formulation for incompressible viscous flows. *Comput Methods Appl Mech Eng*, 29(3):329–349, 1981.

[17] M. Juntunen and R. Stenberg. Nitsche's method for general boundary conditions. *Math. Comp.*, 78(267):1353–1374, 2009.

[18] A. Kazakidi, A. M. Plata, S. J. Sherwin, and P. D. Weinberg. Effect of reverse flow on the pattern of wall shear stress near arterial branches. *Journal of The Royal Society Interface*, 2011.

[19] A. Kazakidi, S.J. Sherwin, and P.D. Weinberg. Effect of reynolds number and flow division on patterns of haemodynamic wall shear stress near branch points in the descending thoracic aorta. *Journal of The Royal Society Interface*, 6(35):539–548, 2009.

[20] H. J. Kim, C. A. Figueroa, T. J. R. Hughes, K. E. Jansen, and C. A. Taylor. Augmented lagrangian method for constraining the shape of velocity profiles at outlet boundaries for three-dimensional finite element simulations of blood flow. *Computer Methods in Applied Mechanics and Engineering*, 198(45-46):3551–3566, 2009.

[21] H. J. Kim, I. E. Vignon-Clementel, C. A. Figueroa, K. E. Jansen, and C. A. Taylor. Developing computational methods for three-dimensional finite element simulations of coronary blood flow. *Finite Elements in Analysis and Design*, 46(6):514–525, 2010.

[22] H. J. Kim, I. E. Vignon-Clementel, C. A. Figueroa, J. F. Ladisa, K. E. Jansen, J. A. Feinstein, and C. A. Taylor. On coupling a lumped parameter heart model and a three-dimensional finite element aorta model. *Annals of Biomedical Engineering*, 37(11):2153–2169, 2009.

[23] J.A. Nitsche. Uber ein variationsprinzip zur lozung von dirichlet-problemen bei verwendung von teilraumen, die keinen randbedingungen unterworfen sind. *Abhandlungen aus dem Mathematischen Seminar der Universitat Hamburg*, 36:9–15, 1970/71.

[24] F. Nobile, M. Pozzoli, and C. Vergara. Time accurate partitioned algorithms for the solution of fluid-structure interaction problems in haemodynamics. *Submitted*, 2011.

[25] F. Nobile and C. Vergara. An effective fluid-structure interaction formulation for vascular dynamics by generalized Robin conditions. *SIAM J. Sci. Comput.*, 30(2):731–763, 2008.

[26] M.S. Olufsen. Structured tree outflow condition for blood flow in larger systemic arteries. *American Journal of Physiology - Heart and Circulatory Physiology*, 276(1 45-1):H257–H268, 1999.

[27] K. Perktold and D. Hilbert. Numerical simulation of pulsatile flow in a carotid bifurcation model. *Journal of biomedical engineering*, 8(3):193–199, 1986.

[28] S. Piperno and C. Farhat. Design of efficient partitioned procedures for transient solution of aerolastic problems. *Rev. Eur. Elements Finis*, 9(6-7):655–680, 2000.

[29] A. Quarteroni and A. Valli. *Numerical approximation of partial differential equations*, volume 23 of *Springer Series in Computational Mathematics*. Springer-Verlag, Berlin, 1994.

[30] A. Veneziani and C. Vergara. Flow rate defective boundary conditions in haemodynamics simulations. *Internat. J. Numer. Methods Fluids*, 47(8-9):803–816, 2005.

[31] A. Veneziani and C. Vergara. An approximate method for solving incompressible Navier-Stokes problems with flow rate conditions. *Comput. Methods Appl. Mech. Engrg.*, 196(9-12):1685–1700, 2007.

[32] C. Vergara. Nitsche's method for defective boundary value problems in incompressible fluid-dynamics. *J. Sci. Comput.*, 46(1):100–123, 2011.

[33] I. E. Vignon-Clementel, C. Alberto Figueroa, K. E. Jansen, and C. A. Taylor. Outflow boundary conditions for three-dimensional finite element modeling of blood flow and pressure in arteries. *Computer Methods in Applied Mechanics and Engineering*, 195(29-32):3776–3796, 2006.

[34] I. E. Vignon-Clementel, C. A. Figueroa, K. E. Jansen, and C. A. Taylor. Outflow boundary conditions for 3d simulations of non-periodic blood flow and pressure fields in deformable arteries. *Computer methods in biomechanics and biomedical engineering*, 13(5):625–640, 2010.

[35] P. E. Vincent, A. M. Plata, A. A. E. Hunt, P. D. Weinberg, and S. J. Sherwin. Blood flow in the rabbit aortic arch and descending thoracic aorta. *Journal of The Royal Society Interface*, 2011.

[36] P.E. Vincent, A.A.E. Hunt, L. Grinberg, S.J. Sherwin, and P.D. Weinberg. A realistic representation of the rabbit aorta for use in computational haemodynamic studies. Number PART B, pages 985–986, 2009.

[37] P. Zunino. Numerical approximation of incompressible flows with net flex defective boundary conditions by means of penalty techniques. *Comput. Methods Appl. Mech. Engrg.*, 198(37-40):3026–3038, 2009.

MOX Technical Reports, last issues

38/2011 PORPORA A., ZUNINO P., VERGARA C., PICCINELLI M.
Numerical treatment of boundary conditions to replace lateral branches in haemodynamics

37/2011 IEVA, F.; PAGANONI, A.M.
Depth Measures For Multivariate Functional Data

36/2011 MOTAMED, M.; NOBILE, F.; TEMPONE, R.
A stochastic collocation method for the second order wave equation with a discontinuous random speed

35/2011 IAPICHINO, L.; QUARTERONI, A.; ROZZA, G.
A Reduced Basis Hybrid Method for the coupling of parametrized domains represented by fluidic networks

34/2011 BENACCHIO, T.; BONAVENTURA, L.
A spectral collocation method for the one dimensional shallow water equations on semi-infinite domains

33/2011 ANTONIETTI, P.F.; BEIRAO DA VEIGA, L.; LOVADINA, C.; VERANI, M.
Hierarchical a posteriori error estimators for the mimetic discretization of elliptic problems

32/2011 ALETTI, G; GHIGLIETTI, A; PAGANONI, A.
A modified randomly reinforced urn design

31/2011 ASTORINO, M.; BECERRA SAGREDO, J.; QUARTERONI, A.
A modular lattice Boltzmann solver for GPU computing processors

30/2011 NOBILE, F.; POZZOLI, M.; VERGARA, C.
Time accurate partitioned algorithms for the solution of fluid-structure interaction problems in haemodynamics

29/2011 MORIN, P.; NOCHETTO, R.H.; PAULETTI, S.; VERANI, M.
AFEM for Shape Optimization